Simulation and theory of hybrid aligned liquid crystal films

TEIXEIRA, P. C. I., BARMES, F., ANQUETIL-DECK, C. and CLEAVER, D. J. <http://orcid.org/0000-0002-4278-0098>

Simulation and theory of hybrid aligned liquid crystal films

P. I. C. Teixeira[1,2], F. Barmes[3], C. Anquetil-Deck[3] and D. J. Cleaver[3]

[1] *Instituto Superior de Engenharia de Lisboa*

Rua Conselheiro Emídio Navarro 1,

P-1950-062 Lisbon, Portugal

[2] *Centro de Física Teórica e Computacional da Universidade de Lisboa*

Avenida Professor Gama Pinto 2,

P-1649-003 Lisbon, Portugal

[3] *Materials and Engineering Research Institute*

Sheffield Hallam University

Pond Street, Sheffield S1 1WB,

United Kingdom

(Dated: 20 November 2008)

Abstract

We present a study of the effects of nano-confinement on a system of hard Gaussian overlap particles interacting with planar substrates through the hard-needle–wall potential, extending earlier work by two of us [D. J. Cleaver and P. I. C. Teixeira, Chem. Phys. Lett. **338**, 1 (2001)]. Here, we consider the case of hybrid films, where one of the substrates induces strongly homeotropic anchoring while the other favours either weakly homeotropic or planar anchoring. These systems are investigated using both Monte Carlo simulation and density-functional theory, the latter implemented at the level of Onsager's second virial approximation with Parsons-Lee rescaling. The orientational structure is found to change either continuously or discontinuously depending on substrate separation, in agreement with earlier predictions by others. Theory is seen to perform well in spite of its simplicity, predicting the positional and orientational structure seen in simulations even for small particle elongations.

PACS numbers: 68.08.-p, 64.70.mf, 61.30.Hn

I. INTRODUCTION

It is often the case, in nature as in human affairs, that the most interesting phenomena occur at boundaries. A fluid in contact with a solid substrate may grow phases that are only metastable in bulk; it may or may not cover that substrate completely; or its constitutent particles may acquire positional order as a result (see, e.g., [1] for a review). If in addition the fluid particles are able to order orientationally, as in liquid crystals (LCs), even richer behaviours may be obtained. Most substrates favour a particular alignment, which is transmitted to the bulk fluid through a mechanism called anchoring [2]. The most common arrangements are homeotropic (i.e., perpendicular to the surface), planar (i.e., parallel to the surface) and tilted. A range of azimuthal anchoring states are also possible. Upon change of experimental conditions, modification of the surface arrangement can be observed to lead to a change in the bulk alignment; such an event is called an anchoring transition [2].

Because they are optically anisotropic, LC materials play a key role in many display technologies (see, e.g., [3]). Typically an LC layer is sandwiched between suitably prepared substrates, which may favour the same (symmetric) or different (hybrid) alignments. An electric field is then used to deviate the orientational order profile from that induced by the substrates alone. Whilst the conventional (and highly successful) twisted-nematic (TN) cell [3] can be thought of as a hybrid geometry, a more recent realisation is the hybrid aligned nematic (HAN) cell of Bryan-Brown *et al.* [4], which has led to a practical realisation of a *bistable* device. Unlike the TN cell, a bistable device has two optically distinct, stable states and an applied voltage is only needed when switching between them. The consequent energy savings are substantial.

Hybrid aligned nanometrically thin LC films have also attracted academic interest. For example, Vandenbrouck *et al.* [5] have observed spinodal dewetting of the nematogen 5CB spun-cast onto silicon wafers. In these experiments, hybrid anchoring was enforced by conflicting boundary conditions: orthogonal at the free surface, and planar at the silicon substrate. Films thicker than 20 nm were found to be stable, while thinner ones broke up into islands which subsequently thickened and merged. This was initially interpreted in terms of competition between elasticity and van der Waals forces [5], though an alternative explanation based on fluctuation-induced interactions was also proposed [6]. Very recently, a more comprehensive experimental study of such systems has been undertaken [7], which

concluded that neither of these theoretical descriptions is robust for film thicknesses below 50 nm. Instead,the authors of [7] called for a theoretical description capable of recognising the molecular structure within such film. We address this directly in this paper.

Applications based on hybrid aligned LC films have also been considered. For example, the Abbott group has investigated the use of hybrid aligned LC films confined between air and water as a novel sensor system [8]. Here, by varying surfactant concentration at the LC-water interface, it has proved possible to switch in and out of the hybrid aligned state, so giving an easy-to-read surfactant detector. Hybrid aligned LC confinement is also pertinent to some of the many fascinating LC colloid systems devised in recent years [9]. Specifically, this is relevant for LC systems loaded either with mixtures of colloidal species with competing surface alignments, or with Janus-type particles [10] featuring competing preferred alignments on different regions of each particle. Such systems have the potential to exhibit qualitatively different particle-particle interactions and self-assembled structures from those observed thus far [11].

In a previous paper [12] we reported computer simulations of a discontinuous structural transition in a thin hybrid film obtained using a hard-particle LC model. Then in [13] we showed how the simple Onsager approximation of density-functional theory (DFT) could provide a semi-quantitatively accurate description of the structure of a fluid of hard rods confined between two hard, impenetrable walls, provided allowance was made, in a phenomenological way, for the incorrect prediction of the location of the isotropic–nematic (I–N) transition. We later applied the same formalism to symmetric films confined between flat substrates of variable penetrability, in order to mimic different anchoring conditions [14], and discussed their relevance in the context of interactions between (large) inclusions in a nematic colloid. Here we return to the more challenging topic of hybrid aligned films, this time comparing simulation outputs with DFT predictions. Our aim is to show that the richer anchoring behaviour of these systems can also be fairly well described by our simple DFT with a standard modification. It was not our intention to perform an exhaustive study of capillary nematisation, adsorption, wetting transitions or other orientationally ordered phases of confined elongated particles. Although such a complete picture is definitely worth pursuing, and DFT is very likely the appropriate tool to arrive at it, the sheer number of relevant variables (pore size, anchoring strengths, density and particle elongation...) mandates a step-by-step approach. Furthermore, notice that we are not (yet) after quantitative

agreement between theory and simulation, since our version of DFT is much too simple.

The remainder of this paper is organised as follows: in section II we recapitulate the model used, and in section III the theory of [13, 14], both modified to allow for unequal anchorings at the confining substrates. We also introduce a simplified form of Parsons-Lee rescaling for a more accurate location of the I–N transition. Then in section IV we present DFT and Monte Carlo (MC) simulation results for the density and order parameter profiles of LC films subject to hybrid anchoring conditions. In particular, we examine the effect of film thickness on whether the structure varies smoothly or discontinuosly on going from one substrate to the other. Finally in section V we discuss the potential and limitations of our approach, and outline some directions for future research.

II. THE MODEL

Following established practise in the field of generic-model LC simulation [15], we consider a purely steric molecular model of elongated particles. Specifically, we take uniaxial rod-shaped particles represented by the hard Gaussian overlap (HGO) potential [16]:

$$U_{12}(\mathbf{r}_{12},\omega_1,\omega_2) = \begin{cases} 0 & \text{if } r_{12} \geq \sigma(\hat{\mathbf{r}}_{12},\omega_1,\omega_2) \\ \infty & \text{if } r_{12} < \sigma(\hat{\mathbf{r}}_{12},\omega_1,\omega_2) \end{cases} , \tag{1}$$

where $\omega_i = (\theta_i, \phi_i)$ are the polar and azimuthal angles describing the orientation of the long axis of particle i, and $\hat{\mathbf{r}}_{12} = \mathbf{r}_{12}/r_{12}$ is a unit vector along the line connecting the centres of the two particles. In this model, the contact distance is that determined by Berne and Pechukas [17] when they considered the overlap of two ellipsoidal Gaussians, given by

$$\sigma(\hat{\mathbf{r}}_{12},\omega_1,\omega_2) = \sigma_0 \left[1 - \frac{1}{2}\chi \left\{ \frac{(\hat{\mathbf{r}}_{12}\cdot\hat{u}_1 + \hat{\mathbf{r}}_{12}\cdot\hat{u}_2)^2}{1+\chi(\hat{u}_1\cdot\hat{u}_2)} + \frac{(\hat{\mathbf{r}}_{12}\cdot\hat{u}_1 - \hat{\mathbf{r}}_{12}\cdot\hat{u}_2)^2}{1-\chi(\hat{u}_1\cdot\hat{u}_2)} \right\} \right]^{-\frac{1}{2}} , \tag{2}$$

where $\hat{u}_i = (\cos\phi_i \sin\theta_i, \sin\phi_i \sin\theta_i, \cos\theta_i)$ and $\chi = (\kappa^2-1)/(\kappa^2+1)$, κ being the particle length to breadth ratio, σ_L/σ_0. For moderate κ, the HGO model is a good approximation to the hard ellipsoid (HE) contact function [18, 19]; furthermore, their virial coefficients (and thus their equations of state, at least at low to moderate densities) are very similar [20]. However, this is no longer true of highly non-spherical particles [16, 21], for which the behaviours of the two models differ appreciably [22]. Finally, HGOs have the considerable computational advantage over HEs that $\sigma(\hat{\mathbf{r}}_{12},\omega_1,\omega_2)$, the distance of closest approach between two particles, is given in closed form [23].

The HGO model is the hard-particle equivalent of the much-studied Gay-Berne model [24]. The phase behaviour of the HGO model is density-driven and fairly simple, comprising only two non-crystalline phases; isotropic and (for $\kappa \gtrsim 3$) nematic fluids at, respectively, low and high number densities $\rho^* = \rho\sigma_0^3$. The isotropic-nematic phase-coexistence densities have been located for various particle elongations in a series of previous MC simulation studies [22, 25, 26]; for the most commonly used elongation of $\kappa = 3$, the transition occurs for $\rho^* \approx 0.30$ with a slight system-size dependence.

Particle–substrate interactions have been modelled, as in [12, 14], by a hard needle–wall (HNW) potential

$$\beta\mathcal{V}^{HNW}(z,\theta) = \begin{cases} 0 & \text{if } |z - z_0^\alpha| \geq \frac{1}{2}\sigma_0\kappa_S\cos\theta \\ \infty & \text{if } |z - z_0^\alpha| < \frac{1}{2}\sigma_0\kappa_S\cos\theta \end{cases} \tag{3}$$

where $\beta = 1/k_{\mathrm{B}}T$ and the z-axis has been chosen to be perpendicular to the substrates, located at $z = z_0^\alpha$ ($\alpha = 1, 2$). $0 \leq \kappa_S \leq \kappa$ sets the length of the needle with which the substrate interacts via $L = \kappa_S\sigma_0$. This affords us a degree of control over the anchoring properties: physically, $0 < L < \sigma_L$ corresponds to a system where the molecules are able to embed their side groups, but not the whole length of their cores, into the bounding walls. Varying L between 0 and σ_L is therefore equivalent to changing the degree of end-group penetrability into the confining substrates. In an experimental situation, this might be achieved by manipulating the density, orientation or chemical affinity of an adsorbed surface layer. The value of L can be set independently at either substrate, or indeed allowed to vary within one or both of the substrates [27]. In this way, symmetric, hybrid and patterned anchoring conditions can all be obtained from this one model. Other choices of wall potential are, of course, possible, which can be derived using the results of [19], and may in some cases be more desirable, e.g., for hard biaxial particles.

We have investigated the HGO+HNW model in a series of previous studies of LCs confined in slab geometry. Our work was preceded by related simulations by Allen [28], in which the particle centres of mass were taken to interact sterically with the substrate (corresponding to the HNW potential with $L = 0$). More recently, a discotic equivalent has been developed by Galindo and co-workers [29]. Finally, we should mention a DFT calculation of the structure of a hybrid aligned HGO film performed by de Vos and Baus [30], for the specific geometry of the TN cell, using the Onsager approximation and Rapini-Papoular-type anchoring potentials [31].

III. THEORY

In order to find the equilibrium density distribution of a HGO film, we start from the grand-canonical functional [32]:

$$\begin{aligned}\beta\Omega\left[\rho(\mathbf{r},\omega)\right] &= \beta\mathcal{F}\left[\rho(\mathbf{r},\omega)\right] + \beta\int\left[\sum_{\alpha=1}^{2}\mathcal{V}^{HNW}(\theta,|z-z_0^\alpha|)-\mu\right]\rho(\mathbf{r},\omega)\,d\mathbf{r}d\omega \\ &= \int\rho(\mathbf{r},\omega)\left[\log\rho(\mathbf{r},\omega)-1\right]\,d\mathbf{r}d\omega \\ &\quad -\frac{\beta F_{HS}^{exc}/N}{8\rho v_0}\int\rho(\mathbf{r}_1,\omega_1)f_{12}(\mathbf{r}_1,\omega_1,\mathbf{r}_2,\omega_2)\rho(\mathbf{r}_2,\omega_2)\,d\mathbf{r}_1d\omega_1d\mathbf{r}_2d\omega_2 \\ &\quad +\beta\int\left[\sum_{\alpha=1}^{2}\mathcal{V}^{HNW}(|z-z_0^\alpha|,\theta)-\mu\right]\rho(\mathbf{r},\omega)\,d\mathbf{r}d\omega, \end{aligned} \tag{4}$$

where $\mathcal{F}\left[\rho(\mathbf{r},\omega)\right]$ is the intrinsic Helmholtz free energy of the inhomogeneous fluid, $f_{12}(\mathbf{r}_1,\omega_1,\mathbf{r}_2,\omega_2) = \exp\left[-\beta U_{12}(\mathbf{r}_1,\omega_1,\mathbf{r}_2,\omega_2)\right]-1$ is its Mayer function, μ is the chemical potential, z_0^α ($\alpha=1,2$) are the positions of the two substrates, and, because we are dealing with hard-body interactions only, for which the temperature is an irrelevant variable, we can set $\beta = 1/k_{\mathrm{B}}T = 1$ in all practical calculations (we retain it in the formulae for generality). $\rho(\mathbf{r},\omega)$ is the density-orientation profile in the presence of the external potential $\mathcal{V}^{HNW}(z,\theta)$; it is normalised to the total number of particles N,

$$\int\rho(\mathbf{r},\omega)\,d\mathbf{r}d\omega = N, \tag{5}$$

and is related to the probability that a particle positioned at $\mathbf{r}$ has orientation between ω and $\omega+d\omega$. From equation (1) it follows that the interaction term in equation (4) is just the excluded volume of two HGO particles, weighted by the density-orientation distributions $\rho(\mathbf{r},\omega)$, The prefactor multiplying this term contains F_{HS}^{exc}, the Carnahan-Starling excess free energy of the reference hard-sphere fluid of the same bulk packing fraction $\eta = \rho v_0 = (\pi/6)\kappa\rho\sigma_0^3$ as the HGO fluid, given by [33]

$$\frac{\beta F_{HS}^{exc}}{N} = \frac{(4-3\eta)\eta}{(1-\eta)^2}. \tag{6}$$

This is a simplified implementation of the Parsons-Lee density re-scaling [34], which amounts to (approximately) summing the higher virial coefficients. In the spirit of [45], this prefactor is a function of the *bulk* density, and not of the *local* density, which should be valid provided the density does not exhibit too sharp spatial variations. Equation (4) is, thus, the 'corrected' Onsager approximation to the free energy of the confined HGO fluid, which we expect

to perform better for particle elongations $\kappa \ll \infty$ inasmuch as structure is determined by location in the phase diagram. We do not expect, however, to see any new structure that is not captured by the Onsager approximation, since what we are doing is a simple density rescaling. More sophisticated approaches exist (see the discussion in section V), but our purpose, as stated above, was to establish just how well we can describe anchoring phenomena using the simplest possible microscopic treatment.

Because the particle-substrate interaction, equation (3), only depends on z and θ, it is reasonable to assume that there is no in-plane structure, so that all quantities are functions of z only. Then equation (4) simplifies to

$$\begin{aligned}\frac{\beta\Omega\left[\rho(z,\omega)\right]}{S_{xy}} &= \int \rho(z,\omega)\left[\log\rho(z,\omega)-1\right]\,dzd\omega \\ &\quad - \frac{\left(1-\frac{3}{4}\eta\right)\eta}{2(1-\eta)^2}\int \rho(z_1,\omega_1)\Xi(z_1,\omega_1,z_2,\omega_2)\rho(z_2,\omega_2)\,dz_1d\omega_1dz_2d\omega_2 \\ &\quad + \beta\int\left[\sum_{\alpha=1}^{2}\mathcal{V}^{HNW}(|z-z_0^\alpha|,\theta)-\mu\right]\rho(z,\omega)\,dzd\omega, \end{aligned} \tag{7}$$

where S_{xy} is the interfacial area. $\Xi(z_1,\omega_1,z_2,\omega_2)$ is now the area of a slice (cut parallel to the bounding plates) of the excluded volume of two HGO particles of orientations ω_1 and ω_2 and centres at z_1 and z_2 [36], for which an analytical expression has been derived [23]. Note that each surface particle experiences an environment that has both polar *and* azimuthal anisotropy, as a consequence of the excluded-volume interactions between the particles in addition to the 'bare' wall potential.

Minimisation of the grand canonical functional, equation (7),

$$\frac{\delta\Omega\left[\rho(z,\omega)\right]}{\delta\rho(z,\omega)} = 0, \tag{8}$$

yields the Euler-Lagrange equation for the equilibrium density-orientation profile,

$$\log\rho(z,\omega) = \beta\mu - \frac{\left(1-\frac{3}{4}\xi\right)}{\left(1-\xi\right)^2}\int' \Xi(z,\omega,z',\omega')\rho(z',\omega')\,dz'd\omega', \tag{9}$$

where the effect of the wall potentials, given by equation (3), has been incorporated through restriction of the range of integration over θ:

$$\int' d\omega = \int_0^{2\pi} d\phi\int_{\pi-\theta_m}^{\theta_m}\sin\theta\,d\theta = \int_0^{2\pi} d\phi\int_{-\cos\theta_m}^{\cos\theta_m} dx, \tag{10}$$

with

$$\cos\theta_m = \begin{cases} 1 & \text{if } |z-z_0^\alpha| \geq \frac{L}{2} \\ \frac{|z-z_0|}{L/2} & \text{if } |z-z_0^\alpha| < \frac{L}{2} \end{cases}, \tag{11}$$

z_0^α being, we recall, the position of substrate α.

It is clear from the structure of equation (9) that μ is the Lagrange multiplier associated with requiring that the mean number of particles in the system be N. We are therefore at liberty to fix either μ or N (see also discussion in [28]): as in earlier work we opt for the latter, since it allows closer contact with (constant NVT) simulation.

Once $\rho(\omega, z)$ has been found, we can integrate out the angular dependence to get the density profile,

$$\rho(z) = \int \rho(z, \omega)\, d\omega, \tag{12}$$

and use this result to define the orientational distribution function (ODF) $\hat{f}(z, \omega) = \rho(z, \omega)/\rho(z)$, from which we can calculate the orientational order parameters in the laboratory-fixed frame [37]:

$$\eta(z) = \langle P_2(\cos\theta)\rangle = Q_{zz}, \tag{13}$$

$$\varepsilon(z) = \langle \sin 2\theta\, \sin\phi\rangle = \frac{4}{3} Q_{yz}, \tag{14}$$

$$\nu(z) = \langle \sin 2\theta\, \cos\phi\rangle = \frac{4}{3} Q_{xz}, \tag{15}$$

$$\varsigma(z) = \langle \sin^2\theta\, \cos 2\phi\rangle = \frac{2}{3}(Q_{xx} - Q_{yy}), \tag{16}$$

$$\tau(z) = \langle \sin^2\theta\, \sin 2\phi\rangle = \frac{4}{3} Q_{xy}, \tag{17}$$

where $\langle \mathcal{A}\rangle = \int \mathcal{A}\hat{f}(z, \omega)\, d\omega$. These are the five independent components of the nematic order parameter tensor, $Q_{\alpha\beta} = \langle \frac{1}{2}(3\hat{\omega}_\alpha\hat{\omega}_\beta - \delta_{\alpha\beta})\rangle$: they give the fraction of molecules oriented along the z-axis (Q_{zz}); along the bisectors of the yz-, xz- and xy-quadrants (Q_{yz}, Q_{xz} and Q_{xy}, respectively); and the difference between the fractions of molecules oriented along the x- and y-axes ($Q_{xx} - Q_{yy}$). In the case under study there is no twist, i.e., the director is confined to a plane that we can take as the xz plane and $\varepsilon(z) = \tau(z) = 0$. The three remaining order parameters, $\eta(z)$, $\nu(z)$ and $\varsigma(z)$, are in general all non-zero owing to surface-induced biaxiality, see our earlier work for $\kappa_S = \kappa$ [13]. This effect has not been neglected in the present treatment, but in what follows we show results for $\eta(z) = Q_{zz}$ only, as we wish to concentrate on the planar-to-homeotropic transition.

IV. RESULTS

We start by calculating the phase diagram of HGOs, to check the quality of the Parson-Lee density re-scaling of Onsager's theory. From the bulk version of equation (7) (i.e., with all spatial integrations extended to $\pm\infty$ and $\mathcal{V}^{HNW}(z,\theta)=0$), we have found the pressure and the chemical potential of the I and N phases and performed the standard double-tangent construction. Both the angle-averaged second virial coefficient (for the I phase) and the angle-dependent excluded volume (for the N phase) are known analytically (see, e.g., [38]). The remaining integrations over ω_i were carried out by 16-point Gauss-Legendre quadrature.

Figure 1 shows the phase diagram, in terms of the reduced density, $\rho^* = \rho\sigma_0^3$, versus elongation, κ; we have also included the Onsager theory results of [13] and coexistence points as determined by Gibbs-Duhem integration [22]. It is seen that, as expected, the present theory performs much better than the earlier one for smaller κ. Both the location and the width of the I–N transition are quantitatively predicted down to $\kappa \approx 5$, and even for $\kappa = 3$ the discrepancy between theory and simulation is only about 10%. This should be contrasted with Onsager theory, which only becomes comparably accurate for $\kappa > 10$. The data of figure 1 are also consistent with the findings of Camp *et al.* [39], who carried out a similar (but more thorough) analysis for the HE fluid. We are, thus, reassured that it is sensible to perform comparison of theory and simulation results for the confined HGO fluid at the same values of the density.

Equation (9) was solved iteratively for $\rho(z,\omega)$ by the Picard method, with an admixture parameter of 0.9 (i.e., 90% of 'old' solution in each iteration), starting from a uniform and isotropic profile. Following Chrzanowska [40], most integrations were performed by Gauss-Legendre quadrature using 64 z-points (the minimum necessary to resolve the structure of the profiles at the higher densities considered) and 16×16 ω-points (for consistency with the bulk calculation).

Note that the range of ω' depends on z': the closer a particle is to a substrate, the fewer orientations are accessible. In order to achieve good accuracy it is nevertheless crucial to include the same number of points in the angular integrations for all z' [40]. Convergence was deemed to have been achieved when the error, defined as the square root of the sum of the squared difference between consecutive iterates at $64 \times 16 \times 16 = 16384$ points), was less than 10^{-3}. The density and order parameter profiles were then calculated from equations

(12) and (13)–(17), respectively.

All simulations were performed in the canonical (NVT) ensemble. The systems were periodic in the x and y directions, along which the simulation box lengths were determined for each imposed number density, ρ^*, through the relationship $L_x = L_y = \sqrt{N/(\rho^* L_z)}$. Typical run-lengths at each state point were 0.5×10^6 MC sweeps (where one sweep represents one attempted move per particle) of equilibration followed by a production run of 0.5×10^6 sweeps. Initial analysis of the surface-induced structural changes has been performed using profiles of the number density, $\rho^*(z)$, the orientational order measured with respect to the substrate normal,

$$Q_{zz}(z) = \frac{1}{N(z)} \sum_{i=1}^{N(z)} \left(\frac{3}{2} u_{i,z}^2 - \frac{1}{2} \right), \tag{18}$$

where $N(z)$ is the instantaneous occupancy of the layer, and the (uniaxial) orientational order parameter in the director frame, $\langle P_2 \rangle(z)$.

Here, we consider two sets of simulations of $\kappa = 3$ HGO particles confined between hybrid-anchoring substrates. First are systems with one strongly homeotropic substrate ($\kappa'_S = 0$) and one which favours either weakly homeotropic ($\kappa'_S = 0.2$), bistable ($\kappa'_S = 0.5$) or planar ($\kappa'_S = 0.8$) alignment. For these, we present data from simulation sequences performed employing $N = 1000$ particles with wall separations $L_z = 4\kappa\sigma_0$. Subsequently, we address systems with one strongly planar substrate and one strongly homeotropic substrate, and investigate the effect of film thickness on the resultant alignment states. Specifically, we consider systems with $L_z = 4\kappa\sigma_0$ and $N = 1000$; $L_z = 6\kappa\sigma_0$ and $N = 1250$; and $L_z = 8\kappa\sigma_0$ and $N = 2000$.

The three sets of $\rho^*(z)$, $Q_{zz}(z)$ and $\langle P_2 \rangle(z)$ profiles obtained for the first of these studies are plotted in figures 2–4. In all cases the interfacial regions at the top (i.e., large-z) substrate ($\kappa'_S = 0.0$) exhibit the features typical of strong homeotropic anchoring, that is a strong density peak immediately at the substrate, with orientational order aligned along the z-axis. At low density ($\rho = 0.28$) the equivalent profiles in the bottom (i.e., small-z) substrate regions correspond reasonably to those substrates' inherent anchoring properties. In both simulation and DFT, these surface effects do not extend into the bulk part of the slab and, therefore, the pairs of interfacial regions exert little influence on one another. As the number density is increased into the bulk nematic phase, however, orientational order develops across the whole of the the cell width, such that the bulk region comes under the

competing influences of both surfaces. We note that, particularly for these thin simulated films, the bulk region order parameter values observed are lower than those found in bulk systems run at given ρ. This arises simply due to the ability of the simulated particles to hide parts of their volume in the substrates, such that the bulk densities achieved in these systems are generally lower than the stated ρ values.

The question naturally arises of whether a true I–N transition still exists in this small ($L_z = 4\kappa\sigma_0$) system. The critical point for capillary nematisation of both hard spherocylinders of length-to-ratio 15 and Zwanzig hard rods was set at around 2 particle lengths by Van Roij *et al.* [41]. On the other hand, Mederos and co-workers [42] did find a critical pore width of about 4 particle lengths, but note that there need be no contradiction between their results and those of Van Roij *et al.*, since the two groups performed calculations/simulations on spherocylinders of very different aspect ratios and used different surface potentials. Our theoretical curves in figures 2 and 3 clearly show two distinct phases, isotropic and nematic, at the lower and higher densities, respectively. At the lower density the order parameter is clearly zero in the central part of the film and the density profile is fairly structureless, unlike at the higher density. Admittedly the nematic phase is not very strongly ordered and the pore width may be subcritical.

In two of the three cases considered ($\kappa'_S = 0.2$ and $\kappa'_S = 0.5$), the profiles indicate a smooth transition between the two surface arrangements, with little variation in $\langle P_2 \rangle(z)$ and almost linear changes in $\rho^*(z)$ and $Q_{zz}(z)$ being seen in the bulk regions. For $\kappa'_S = 0.8$, however, there is a clear drop in $\langle P_2 \rangle(z)$ in a localised z-range which suggests a discontinuity, perhaps somewhat rounded because the system is probably subcritical, see discussion in preceding paragraph. This is consistent with the configuration snapshots of figure 5: the low values of $\langle P_2 \rangle(z)$ might be understood by the presence of particles with very different orientations in the same slice (although one should be careful not to read too much into an instantaneous configuration). This effect is not apparent from the $Q_{zz}(z)$ profile, though, as similar values could be obtained from a slice of n particles with $\theta \sim \pi/4$ and a slice of equal number of particles with $\theta \sim 0$ and $\theta \sim \pi/2$. If real, the above discontinuous transition is similar to that reported earlier by two of us [12]: in both cases, when the anchorings at the two walls are of very different strengths then the tilt angle varies smoothly (as in figures 2 and 3), but when they are of comparable strengths then there is a transition to a regime where the tilt angle does not vary smoothly (as in figure 4). Note that it is essential that films be sufficiently

thin in order to exhibit this kind of behaviour [43, 44]; the qualitative dependance on film thickness will be discussed later.

Overall agreement between theory and simulation is good at the lower density for all needle lengths. At the higher density, theory succeeds in capturing both the positional and orientational structure observed in the simulated films. However, quantitative agreement deteriorates somewhat as the film anchorings are made more hybrid, i.e., as the bottom wall κ'_S value is increased. When this parameter is set at $\kappa'_S = 0.2$, the heights and numbers of peaks/troughs are fairly well predicted, but their positions are slightly shifted. For $\kappa'_S = 0.5$, the theory predicts a somewhat more structured density, and a higher degree of orientational order, in the lower half of the film (adjacent to the bistable wall) than is present in the simulation data. Then for $\kappa'_S = 0.8$ agreement again improves throughout the system. The fact that the second and third density peaks (and corresponding features in the order parameter profiles) from theory are systematically shifted away from the substrates is probably a consequence of an overestimation of the strength of the nematic phase.

Next, we consider systems in which the substrate conditions were held fixed at strongly planar ($\kappa'_S = 1.0$) and strongly homeotropic ($\kappa'_S = 0.0$,) but the film thickness was varied. This required increasing the number of particles in the system, in order to avoid interactions between particles and their images. We took $L_z = 4\kappa\sigma_0$, $L_z = 6\kappa\sigma_0$ and $L_z = 8\kappa\sigma_0$, and $N = 1000$, $N = 1250$ and $N = 2000$, respectively. For the largest of these the number of z-points in the DFT calculation also had to be increased to 100, and Gauss-Chebyshev quadrature was used. Typical profiles obtained at the nominally nematic density of $\rho^* = 0.35$ are shown in figure 6 where, for comparison purposes, the z coordinates have been scaled by L_z.

Not surprisingly, both theory and simulation predict that the discontinuous director field observed for the $\kappa'_S = 0.8$ system above is also exhibited by the thinnest of these strongly anchored systems. This is most clearly apparent from the marked minima seen in the corresponding $\langle P_2 \rangle(z)$ profiles. For the two thicker systems, however, theory and simulation are in disagreement; theory continues to predict the discontinuous behaviour, whereas the simulations exhibit bent director arrangements in which the director varies smoothly from planar to homeotropic as the film is traversed. The profiles obtained for these continuous bent director arrangements are characterised by extended regions in the bulk of the confined films in which the density and nematic order profiles are virtually flat, while the $Q_{zz}(z)$ profile

varies linearly. Indeed, when plotted in terms of the scaled length z/L_z it is striking that these two $Q_{zz}(z)$ profiles are effectively identical away from the structural oscillations at each wall. The bent director structures represented by these profiles are exhibited particularly clearly by the associated configuration snapshots shown in figure 7.

The observation of two distinct profile structures in these simulations is consistent with there being a critical film thickness at which the transition between the two arrangements takes place. For this particular set of wall-particle interaction parameters, this critical thickness appears to lie between $4\kappa\sigma_0$ and $6\kappa\sigma_0$. This result places a finite limit on the theoretical prediction [43, 44] that hybrid-anchored films with a thickness of only a few molecular lengths do not exhibit a continuous bent-director structure. It is also consistent with the experimental observation of Vanderbrouck *et al.* [5] that thin films of 5CB spun-cast onto a silicon wafer, and thus having hybrid anchoring conditions, are stable only if their thickness is greater than 20 nm.

In contrast, our DFT was not able to recover the continuous bend configuration for these systems: all theory $\langle P_2 \rangle(z)$ profiles exhibit a region of depressed order in the bulk, which shrinks in extension as L_z increases, but is still present in the thickest film, $L_z = 8\kappa\sigma_0$. Comparing the DFT and simulation profiles here, it is evident that the density oscillations given by DFT are somewhat overestimated, with peak positions systematically shifted farther away from the substrates than those found in the equivalent simulations. This suggests that theory overestimates the extent of the positional structure adopted by these systems. The failure to observe a critical thickness here is certainly consistent with the notion that the effective anchoring strengths pertinent to the DFT systems are greater than those in the simulation systems. Since anchoring strength emerges from complex many body packing and layering effects, however, it is not surprising that our second-virial level DFT has this property.

V. CONCLUSIONS

In this paper we have presented a combined MC simulation and DFT treatment of a HGO hybrid aligned fluid confined between parallel substrates. The anchoring can be tuned independently at either substrate, by varying the extent to which a particle is allowed to penetrate it. The Onsager approximation, combined with a simple Parsons-Lee density

re-scaling, can in some cases yield semi-quantitative predictions for the density and orientational distribution of particles of elongation as small as $\kappa = 3$. Many of our profiles exhibit fairly strong oscillations, which are indicative of layering phenomena and are expected if the demsity is not very low, i.e., deeper into the N phase than the immediate vicinity of the I–N transition. The same qualitative behaviour was reported by Mederos *et al.* [42], who went deep into the N phase, but not by Van Roij *et al.* [41], who were interested mostly in the I–N transition. Neither of these sets of authors, however, considered hybrid aligned films as we do here. Furthermore, the solution procedure also yields the free energy, thus making it possible to derive the effective interaction between substrates. This will be the subject of future work. More sophisitcated theoretical approaches are of course available, such as a weighted-density [45] or fundamental-measure [46] approximation, which would very likely be more accurate, but are also highly non-trivial to implement.

The current theory appears very able to capture the complex positional and orientational structure adopted within the thin LC films considered here. As such, it represents a significant advance of the type recently called for by Delabre and co-workers [7]. In the systems we investigated, the theory appears able to describe the discontinuous structural transition between the two main hybrid-anchored states, although the critical thickness is overestimated. This latter point is to be expected though, as this thickness depends crucially on the anchoring strengths at the two substrates. More precise tuning of this would require direct calculation of the HNW anchoring energy, along the lines of the studies reported in [28] and [47]. The possible interplay between this and a capillary nematisation transition also needs to be investigated by mapping the full phase diagram of the confined fluid.

Finally, we note that the theory presented here can be straightforwardly generalised to more sophisticated confinement geometries or surface interactions, and also to mixtures of two or more types of hard body. As such, it could be used to determine effective inter-particle interactions for a range of colloid-in-LC suspensions. One can alternatively envisage the same approach being used to study the potentially very rich behaviour of a confined binary LC mixture in which the two components have different easy axes at either substrate. This work is in progress and will be reported elsewhere.

Acknowledgements

We wish to acknowledge useful discussions with C. M. Care and J. R. Henderson. This work has benefitted from financial support from Sheffield Hallam University and the British Council's Treaty of Windsor programme, grant no. B-54/07.

---

[1] See, e.g., articles by D. Beaglehole, T. J. Sluckin and A. Poniewierski, and D. E. Sullivan and M. M. Telo da Gama, in *Fluid Interfacial Phenomena*, ed. by C. A. Croxton (Wiley, Chichester, 1986).

[2] B. Jérôme, Rep. Prog. Phys. **54**, 391 (1991).

[3] See, e.g., T. J. Sluckin, Contemp. Phys. **41**, 37 (2000).

[4] G. P. Bryan-Brown, E. L. Wood and I. C. Sage, Nature **399**, 338 (1999).

[5] F. Vandenbrouck, M. P. Valignat and A. M. Cazabat, Phys. Rev. Lett. **82**, 2693 (1999).

[6] P. Ziherl, R. Podgornik and S. Žumer, Phys. Rev. Lett. **84**, 1228 (2000); P. Ziherl, F. K. P. Haddadan, R. Podgornik and S. Žumer, Phys. Rev. E **61**, 5361 (2000).

[7] U. Delabre, C. Richard, G. Guéna, J. Meunier and A.-M. Cazabat, Langmuir **24**, 3998 (2008).

[8] N. A. Lockwood and N. L. Abbott, Current Opinion in Coll. Interf. Sci. **10**, 111 (2005).

[9] P. Poulin, H. Stark, T. C. Lubensky and D. A. Weitz, Science 275, 1770 (1997).

[10] B. P. Binks and P. D. I. Fletcher, Langmuir **17**, 4708 (2001).

[11] D. Antypov and D. J. Cleaver, J. Phys.: Condens. Matter **16**, S1887 (2004).

[12] D. J. Cleaver and P. I. C. Teixeira, Chem. Phys. Lett. **338**, 1 (2001).

[13] A. Chrzanowska, P. I. C. Teixeira, H. Eherentraut and D. J. Cleaver, J. Phys.: Condens. Matter **13**, 4715 (2001).

[14] P. I. C. Teixeira, F. Barmes and D. J. Cleaver, J. Phys.: Condens. Matter **16**, S1969 (2004).

[15] C. M. Care and D. J. Cleaver, Rep. Prog. Phys. **68**, 2665 (2005).

[16] M. Rigby, Molec. Phys. **68**, 687 (1989).

[17] B. J. Berne and P. Pechukas, J. Chem. Phys. **56**, 4213 (1972).

[18] J. W. Perram and M. S. Wertheim, J. Comput. Phys. **58**, 409 (1985); J. W. Perram, J. Rasmussen, E. Praestgaard and J. L. Lebowitz, Phys. Rev. E **54**, 6565 (1996).

[19] M. P. Allen, G. T. Evans, D. Frenkel and B. M. Mulder, Adv. Chem. Phys. **86**, 1 (1993).

[20] V. R. Bhethanabotla and W. Steele, Molec. Phys. **60**, 249 (1987).

[21] S. L. Huang and V. R. Bhethanabotla, Int. J. Mod. Phys. C **10**, 361 (1999).

[22] E. de Miguel and E. Martín del Rio, J. Chem. Phys. **115**, 9072 (2001).

[23] E. Velasco and L. Mederos, J. Chem. Phys. **109**, 2361 (1998).

[24] J. G. Gay and B. J. Berne, J. Chem. Phys. **74**, 3316 (1981).

[25] P. Padilla and E. Velasco, J. Chem. Phys. **106**, 10299 (1997).

[26] E. de Miguel and E. Martín del Rio, J. Chem. Phys. **118**, 1852 (2003).

[27] J. P. Bramble, S. D. Evans, J. R. Henderson, C. Anquetil, D. J. Cleaver and N. J. Smith, Liq. Cryst. **34**, 1059 (2007).

[28] M. P. Allen, Molec. Phys. **96**, 1391 (1999); J. Chem. Phys. **112**, 5447 (2000).

[29] M. M. Pineiro, A. Galindo and A. O. Parry, Soft Matter **3** 768 (2007).

[30] T. de Vos and M. Baus, J. Chem. Phys. **128**, 194903 (2008).

[31] A. Rapini and M. Papoular, J. Phys. Colloq. **C4**, **30**, 54 (1969).

[32] R. Evans, Adv. Phys. **28**, 143 (1979).

[33] N. F. Carnahan and K. E. Starling, J. Chem. Phys. **51**, 635 (1969).

[34] J. D. Parsons, Phys. Rev. A **19**, 1225 (1979); S. D. Lee, J. Chem. Phys. **78**, 4972 (1987).

[35] D. de las Heras, L. Mederos and E. Velasco, Phys. Rev. E **68**, 031709 (2003).

[36] A. Poniewierski, Phys. Rev. E **47**, 3396 (1993).

[37] M. M. Telo da Gama, Molec. Phys. **52**, 585 (1984); *ibid.* **52**, 611 (1984).

[38] E. Velasco, A. M. Somoza and L. Mederos, J. Chem. Phys. **102**, 8107 (1995).

[39] P. J. Camp, C. P. Mason, M. P. Allen, A. A. Khare and D. A. Kofke, J. Chem. Phys. **105**, 2837 (1996).

[40] A. Chrzanowska, J. Comput. Phys. **191**, 265 (2003).

[41] R. van Roij, M. Dijkstra and R. Evans, Europhys. Lett. **49**, 350 (2000); J. Chem. Phys. **113**, 7689 (2000); M. Dijkstra, R. van Roij and R. Evans, Phys. Rev. E **63**, 051703 (2001).

[42] D. de las Heras, E. Velasco and L. Mederos, J. Chem. Phys. **120**, 4949 (2004); Phys. Rev. E **74**, 011709 (2006).

[43] G. Barbero and R. Barberi, J. Phys. (Paris) **44**, 609 (1983).

[44] A. Šarlah and S. Žumer, Phys. Rev. E **60**, 1821 (1999).

[45] A. M. Somoza and P. Tarazona, J. Chem. Phys. **91**, 517 (1989); E. Velasco, L. Mederos and D. E. Sullivan, Phys. Rev. E **62**, 3708 (2000).

[46] G. Cinacchi and F. Schmid, J. Phys.: Condens. Matter **14**, 12189 (2002).

[47] D. Andrienko and M. P. Allen, Phys. Rev. E **66**, 021704 (2002).

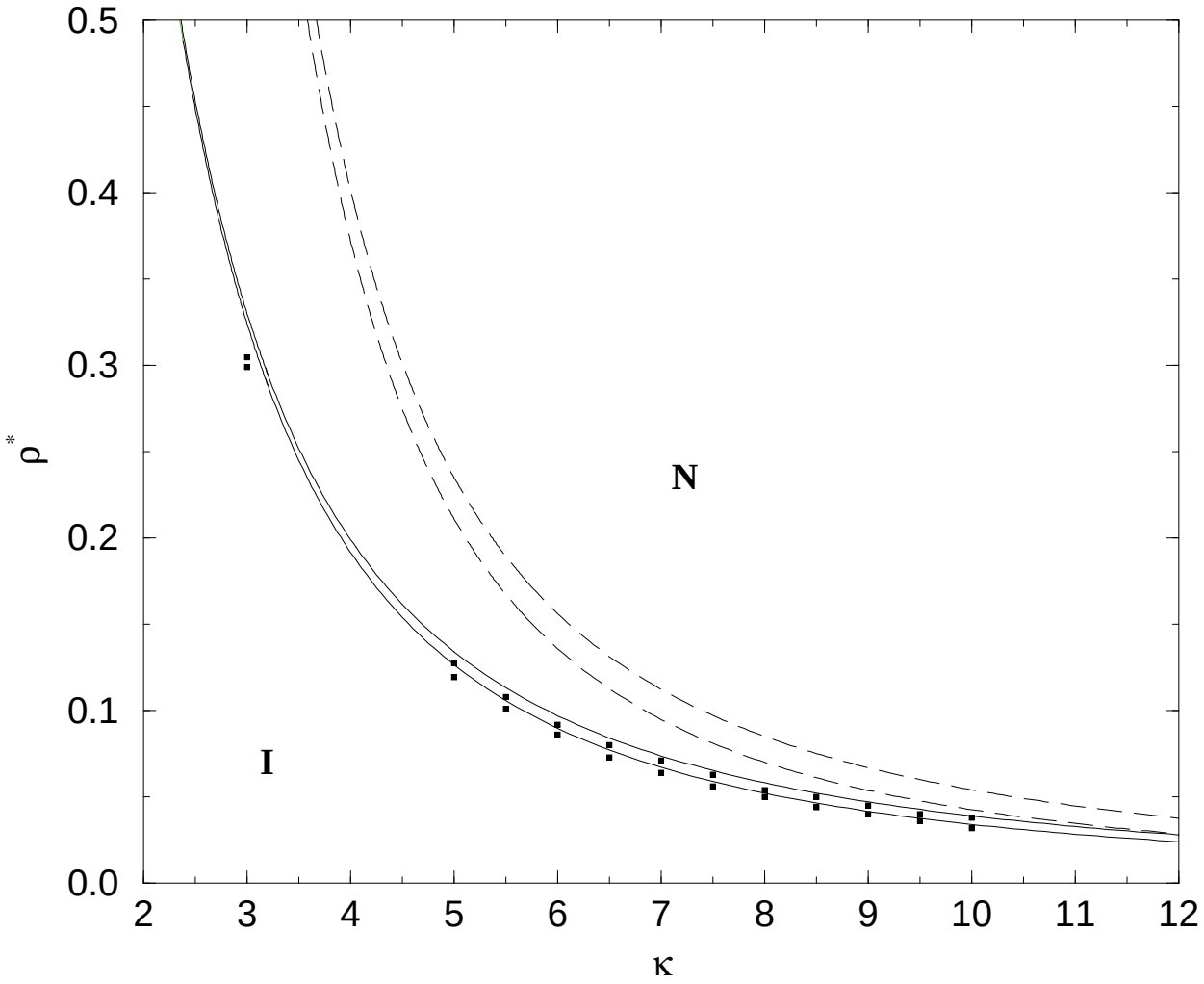

FIG. 1: I–N phase diagram of the HGO fluid: $\rho^* = \rho\sigma_0^3$ and κ are the reduced density and the elongation, respectively. Solid lines: Onsager theory with Parsons-Lee density re-scaling; dashed lines: Onsager theory [13]; filled squares: MC simulation results [22].

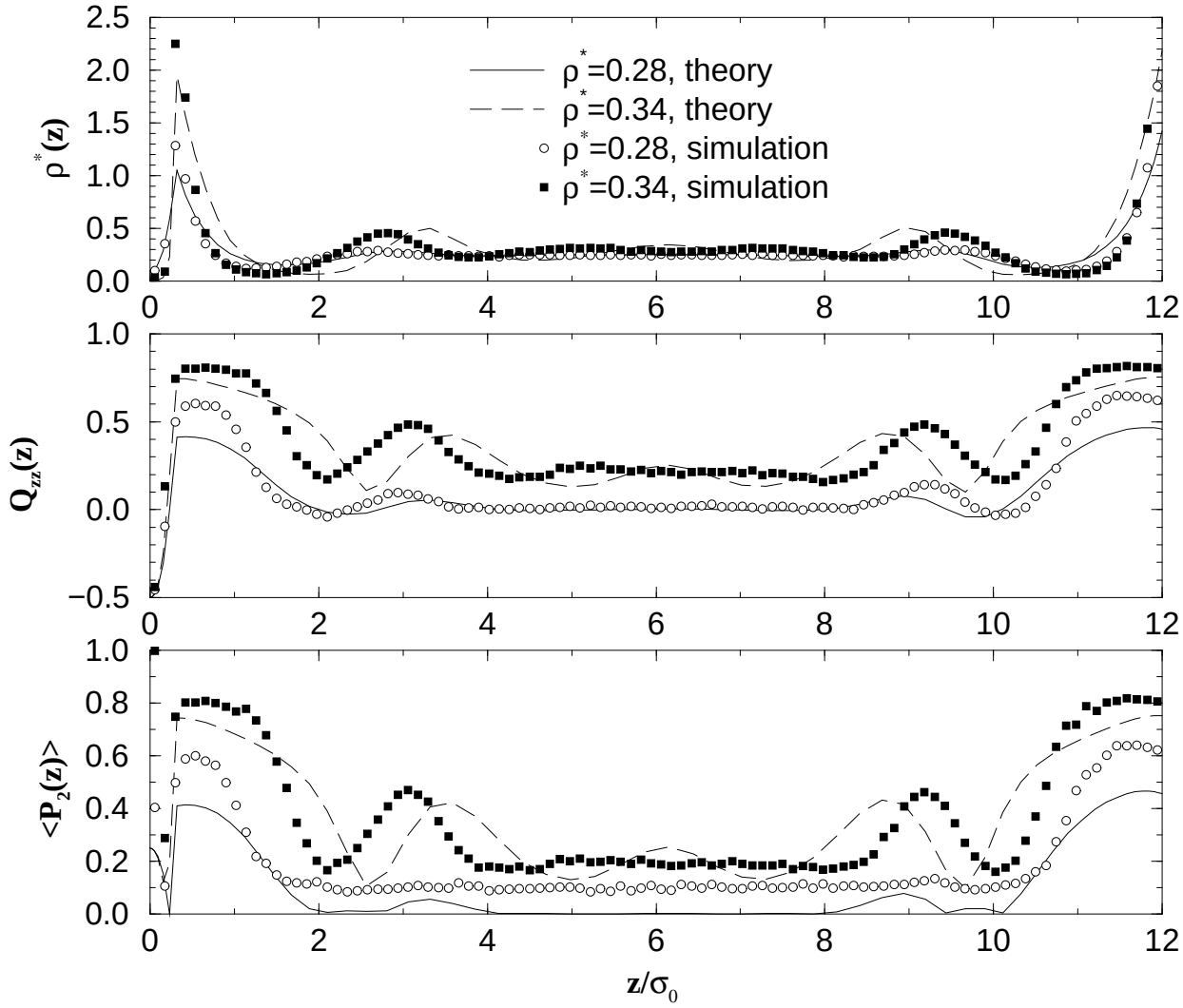

FIG. 2: Reduced density $\rho^*(z)$ (top), order parameter $Q_{zz}(z)$ (middle) and order parameter $\langle P_2 \rangle(z)$ (bottom) profiles for a hybrid film of HGO particles of elongation $\kappa = 3$, needle length $\kappa'_S = 0.2$ on the small-z (or bottom) substrate and $\kappa'_S = 0.0$ on the large-z (or top) substrate, for $\rho^*_{bulk} = 0.28$ (solid line and open circles) and $\rho^*_{bulk} = 0.34$ (dashed line and filled squares). Lines are from theory, symbols are from simulation. The lower density lies in the I phase, the higher density in the N phase See the text for details.

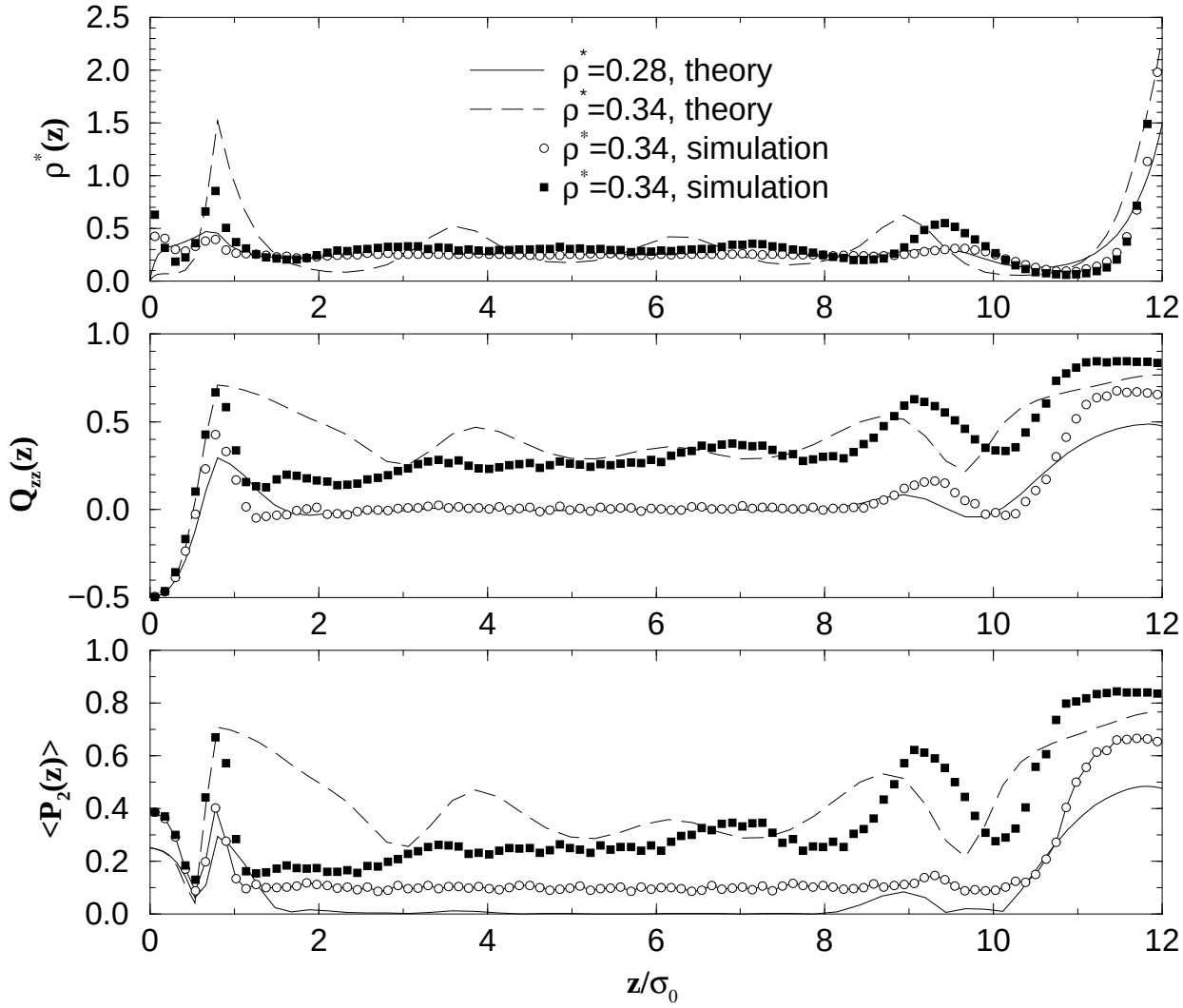

FIG. 3: Same as figure 2, but for $\kappa_S' = 0.5$ at the small-z substrate.

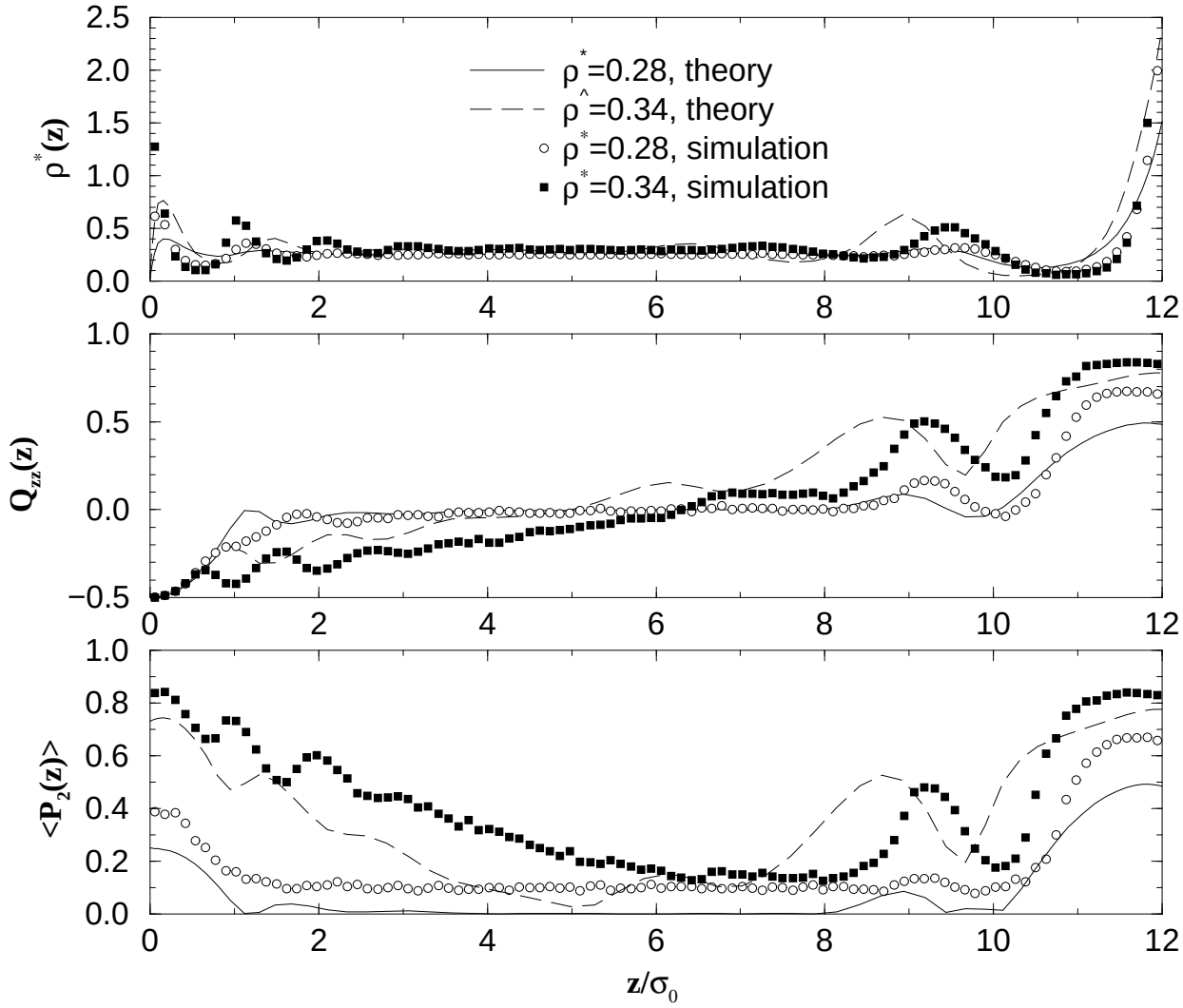

FIG. 4: Same as figures 2 and 3, but for $\kappa'_S = 0.8$ at the small-z substrate.

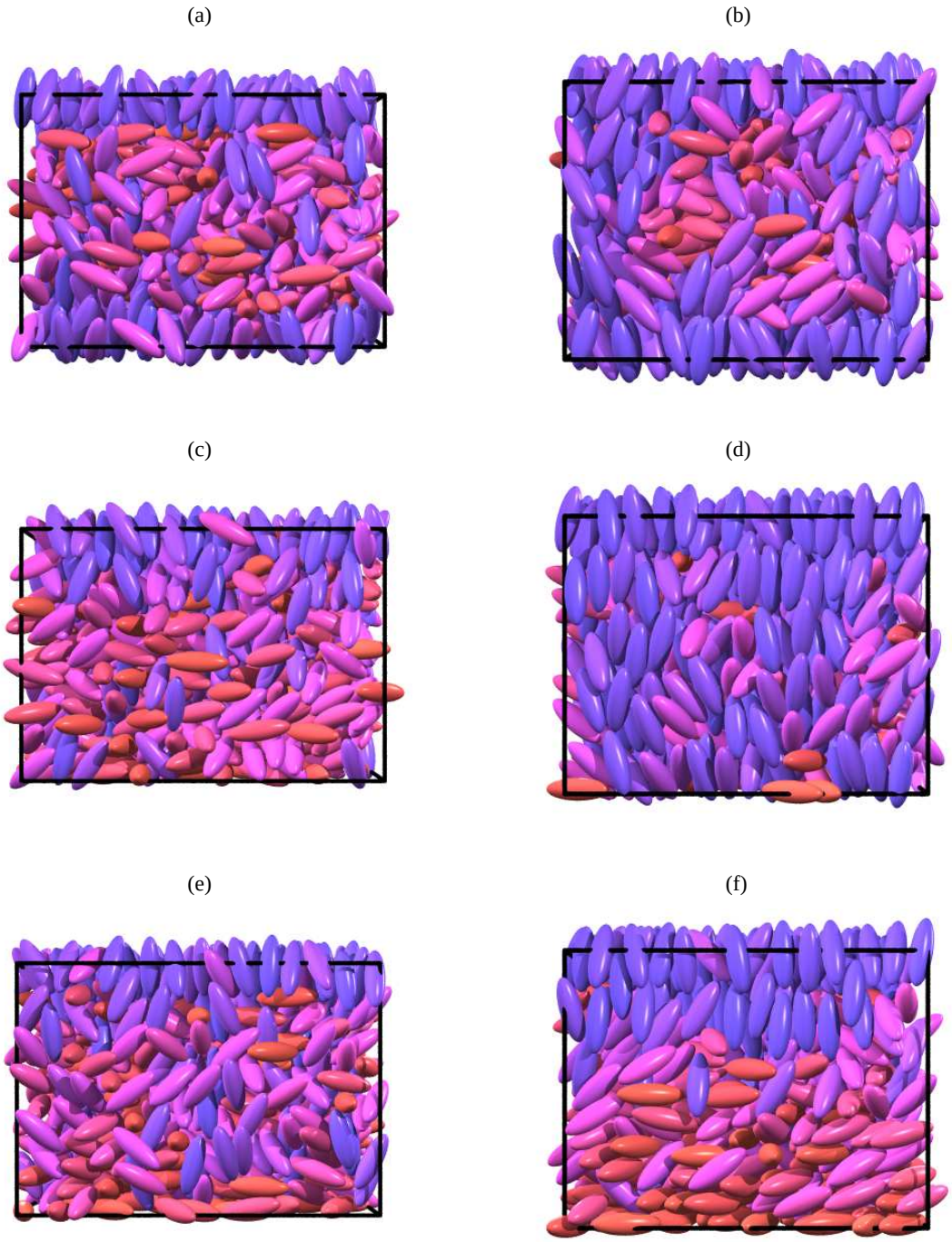

FIG. 5: Configuration snapshots for hybrid films with strong homeotropic anchoring at the top substrate ($\kappa'_S = 0.0$). Bottom substrate: (a) and (b) weakly homeotropic ($\kappa'_S = 0.2$); (c) and (d) bistable ($\kappa'_S = 0.5$); (e) and (f) planar ($\kappa'_S = 0.5$). Snapshots (a), (c) and (e), on the left, correspond to the bulk isotropic phase ($\rho^* = 0.28$); (b), (d) and (f), on the right, to the bulk nematic phase ($\rho^* = 0.34$).

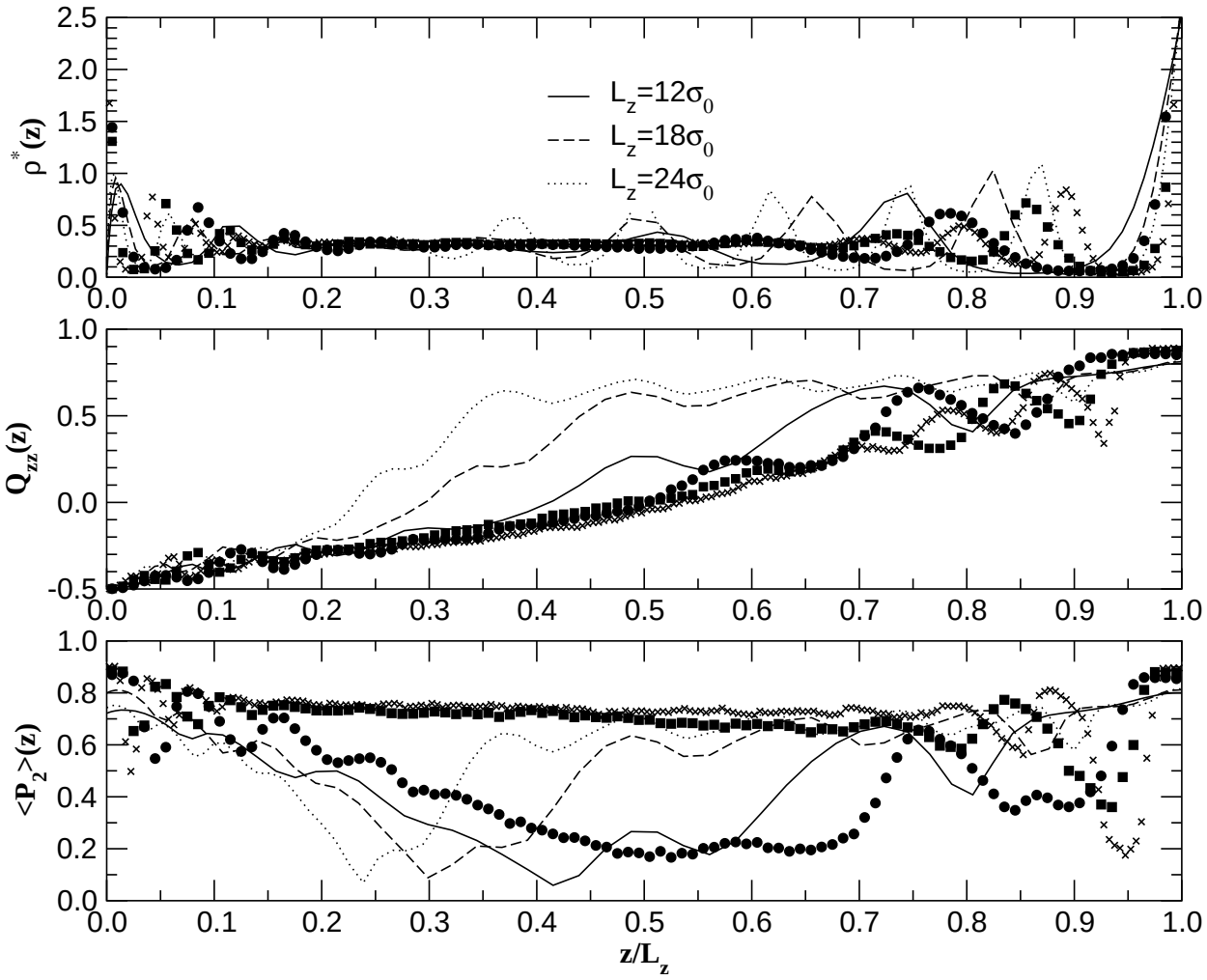

FIG. 6: Reduced density $\rho^*(z)$ (top), order parameter $Q_{zz}(z)$ (middle) and order parameter $\langle P_2 \rangle(z)$ (bottom) profiles for a hybrid film of HGO particles of elongation $\kappa = 3$, needle length $\kappa'_S = 1.0$ on the small-z (bottom) substrate and $\kappa'_S = 0.0$ on the large-z (top) substrate, for $\rho^*_{bulk} = 0.35$. Solid line and open circles: $L_z = 4\kappa\sigma_0$; dashed line and filled squares: $L_z = 6\kappa\sigma_0$; dotted line and crosses: $L_z = 8\kappa\sigma_0$. Lines are from theory, symbols are from simulation.

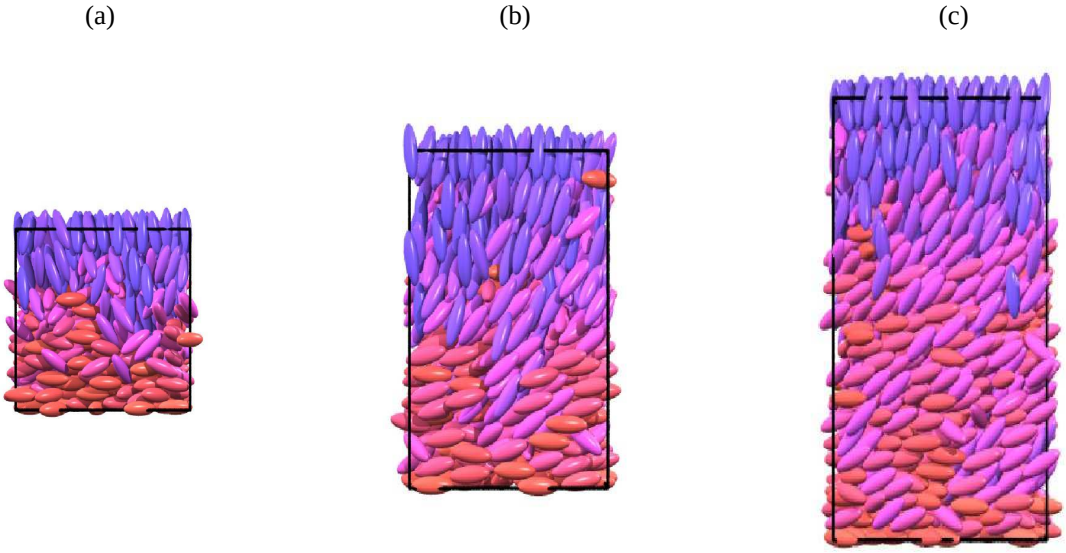

FIG. 7: Typical configuration snapshots of hybrid films HGO particles of elongation $\kappa = 3$, using the HNW surface potential with $\kappa'_S = 1.0$ (bottom) and $\kappa'_S = 0.0$ (top). (a) $L_z = 4\kappa\sigma_0$ and $N = 1000$ particles, (b) $L_z = 6\kappa\sigma_0$ and $N = 1250$ particles, and (c) $L_z = 8\kappa\sigma_0$ and $N = 2000$ particles. In all cases $\rho^*_{bulk} = 0.35$.